CONF-9109286--2

DE92 000431

Invited paper for the E-MRS *Summer School on*
Laser Ablation of Electronic Materials: Basic Mechanisms and
Applications, Carcans-Maubuisson, France (ed. by
E. Fogarassy, S. Lazare, and J. Narayan, Elsevier/North Holland, 1991)

EFFECTS OF AMBIENT BACKGROUND GASES ON YBCO PLUME PROPAGATION UNDER FILM GROWTH CONDITIONS: SPECTROSCOPIC, ION PROBE, AND FAST PHOTOGRAPHIC STUDIES

David B. Geohegan

September 1991

Solid State Division
Oak Ridge National Laboratory
P. O. Box 2008
Oak Ridge, Tennessee 37831-6056

managed by
MARTIN MARIETTA ENERGY SYSTEMS, INC.
for the
U.S. DEPARTMENT OF ENERGY
under contract DE-AC05-84OR21400

EFFECTS OF AMBIENT BACKGROUND GASES ON YBCO PLUME PROPAGATION UNDER FILM GROWTH CONDITIONS: SPECTROSCOPIC, ION PROBE, AND FAST PHOTOGRAPHIC STUDIES

David B. Geohegan

Solid State Division, Oak Ridge National Laboratory,
Oak Ridge, TN 37831-6056 USA

Abstract

The formation, composition, and propagation of KrF laser-produced plasmas from $Y_1Ba_2Cu_3O_{7-x}$ have been studied with emphasis on topics relevant to film growth by pulsed-laser deposition. Spatially and temporally resolved, high-resolution optical absorption and emission spectroscopy, fast ion probes, and fast photography [obtained with a gated, image-intensified CCD array detector (ICCD)] are employed to investigate both emitting and non-emitting species in the laser plume as well as the overall shape and propagation of the laser plasma in background gases of oxygen and xenon.

Transient optical absorption spectroscopy is applied to study the composition of the plume of ejected material from the dense layer near the target surface to distances of several centimeters. Optical absorption persists long after the decay of plasma fluorescence, indicating a slower component to plume transport. The absorption of YO formed by YBCO ablation in vacuum and by-yttrium ablation in oxygen is presented.

Fast electric ion probes are utilized to measure velocities and total collected charge of the positive ions in the expanding YBCO laser plasma from near-threshold, vacuum conditions into the high fluence, background gas conditions utilized for thin-film growth. The exponential attenuation of the positive ion flux transmitted through 50–300 mTorr background oxygen is measured and used to define an attenuation coefficient.

The slowing of the laser plasma and formation of shock structures due to gas collisions is studied by ion probe measurements and fast ICCD photography. A comparison between shock wave propagation and drag models is presented to describe the arrival time and shape of the ion probe current waveform with distance.

1. INTRODUCTION

Laser ablation for in situ film growth of the high-T_c superconductors requires the presence of background oxygen during deposition to maintain the proper crystalline phase throughout deposition. The ejected plume of material is scattered and attenuated by this background oxygen, forming oxides and possibly clusters which may aid oxygen incorporation in the growing film. During the trip from target to substrate, ablated atoms and ions from YBCO are accelerated to most probable initial kinetic energies of ~40–70 eV within 1 mm of the target[1] and then thermalized over a distance of several centimeters.[2] For film growth, background gas pressures and laser energies are balanced to maintain the correct phase, provide an adequate deposition rate, assure stoichiometry transfer, and limit the incident kinetic energies to a desirable range.

The interaction of the ablation plume with ambient background gases is obviously a complex hydrodynamic problem which is receiving renewed attention due to its importance to pulsed-laser deposition.[3–7] The starting point is the hot, high-pressure plasma at the surface of the target. At very low pressures, the supersonic free expansion of the ejected material sweeps up the background gas with little change in momentum.[8] At very high background pressures, however (where the mass of ablated products is small compared to the mass of gas set in motion by the plume), the kinetic energy of the plume ejectants is transferred to a shock wave which propagates through the background gas.[9,10] Intermediate to these two extremes lies the film growth regime.

For film growth, a fraction of the ablated products are required to penetrate the background gas, and considerable energy is expended during the collisions. Initially the pressure in the dense plume is greater than the ambient pressure. During the initial phase of expansion, one might expect the plume to push the background gas ahead and aside, the background gas acting as a viscous force on a moving object. As the plume expands and cools, its pressure decreases rapidly. At higher pressures, as the background gas gains increasingly more momentum from the plume, a transition to the shock regime might be expected.

A variety of reactive collisions depend upon the interaction between the plume and background gas. The formation of oxides and clusters are two examples. In order to optimize formation of these products, a knowledge of how the plume material interacts with the background gas is essential.

In this paper, the effects of ambient background gases on the propagation of laser-produced plasmas of YBCO are explored. The thermalization and attenuation of the propagating plasma are investigated with fast ion probes which detect the flux of positive ions transmitted through the gas. Fast-exposure (5–20 ns) two-dimensional CCD array images of the visible plume fluorescence provide progressive images of the plume expansion for comparison with the ion probe and spectroscopic measurements. The results are compared to two models: a drag force model and a shock wave propagation model. The presence of YO in the ablated plume close to the pellet in vacuum and far from the pellet following gas phase reactions are temporally resolved by optical absorption spectroscopy.

2. EXPERIMENTAL

Most elements of the experimental apparatus have been described before.[2,6,11] The configuration for the experiments described below is outlined in Fig. 1. A high-density $Y_1Ba_2Cu_3O_{7-x}$ pellet (W. R. Grace Co.) was rotated near the center of a 16"-diam vacuum chamber. The central portion of a Lambda Physik EMG 210 excimer laser beam was apertured to typically ~1 cm^2 and focused by a single spherical or cylindrical lens to either a square or a line on the target surface at an incident angle of 30° from below. Energy densities were varied by reflection losses from a stack of Suprasil plates before the first aperture.

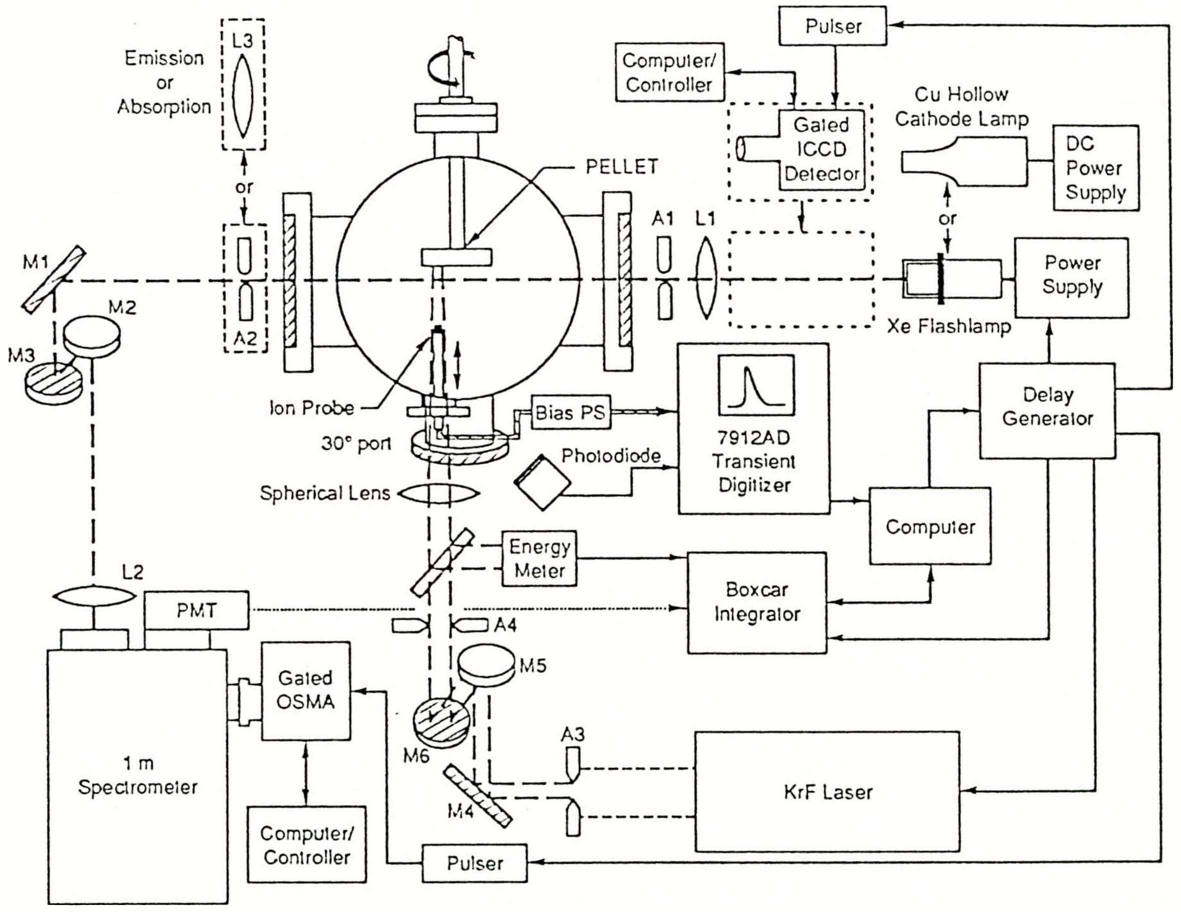

Figure 1: Experimental apparatus used for optical absorption, optical emission, ion probe, and gated ICCD measurements of laser-produced plasma plumes.

Optical emission and absorption of the laser plume were spectrally resolved by a 1-m air path spectrometer with 2400 g/mm grating, providing 0.01 Å resolution. The plume region was imaged onto the entrance slits of the spectrometer, sampling a vertical slice corresponding to ~50 μm of the horizontally expanding plume. In addition, a gated, intensified diode array (Princeton Instruments IRY-700RB) was utilized to record simultaneously plasma emission over 50-Å-wide spectral regions with variable delays and adjustable gate widths >3.8 ns. A fast (0.3-ns) photomultiplier provided temporal histories of a selected emission or absorption line to the transient digitizer for storage or the boxcar integrator for signal averaging during a spectral scan. A pulsed Xe flashlamp provided a structured continuum for the absorption measurements.

A cylindrical copper Langmuir probe or, alternatively, a copper planar probe housed 2 mm behind a Cu plane with 0.02 cm^2 aperture were both employed for measurements of the positive ion flux along the target normal. The ion probe was floated with respect to the chamber and pellet by terminating the coaxial signal line at the digitizer and by providing the bias with a completely isolated and shielded 1-mfd-capacitor-bypassed 300-V battery and potentiometer in series with the 50 ohm signal line. The probes were operated at saturation in the electron-repelling regime with typically -100-V bias.

Fast, side-on views of the plume expansion were made by recording the overall visible emission from the plasma plume with a gated, intensified CCD camera system (Princeton Instruments ICCD576G/RB). A 105-mm Nikon telephoto lens imaged a region extending ~4.5 cm normal to the pellet onto the detector surface. The detector utilizes a microchannel plate (MCP) which prevents photoelectrons from the photoemissive detector surface from reaching the phosphor/CCD array until a gate voltage pulse is applied. Fast (3.8-ns or longer) gate pulses (acting as the shutter for the camera) were supplied at variable times after the firing of the laser for "stop-action" images of the plume expansion. The MCP provides amplification and sensitivity beyond that of regular photography, allowing fainter images such as those found in the lower background gas pressures explored here to be captured.

It is important to note that the exposure chosen for the ICCD images is as difficult a problem as in ordinary photography. Overexposure loses detail in bright regions of interest while underexposure misses the fainter regions. For each exposure in these experiments, the gain on the MCP was set just short of saturation, to utilize the maximum dynamic range. The 14-bit dynamic range of each pixel on the 378 x 584 CCD array was digitized and stored to be processed later with image processing software (Signal Analytics-IP Lab).

3. INITIAL EXPANSION IN VACUUM REVIEW

In the early stages of expansion, the hot plasma at the pellet emits continuum fluorescence from free-free transitions. In high resolution, spectral lines from neutrals and singly charged ions display Stark broadening arising from collisions between the electrons and ions with atoms. The plasma quickly relaxes into the ground states of the atoms and ions. During this time, resonance line fluorescence, such as shown in Fig. 2 for Ba^+ ions above a YBCO target, displays broad wings with a sharper absorption feature at line center. This indicates a shell structure to the plasma, with a very hot emitting central region and a ground state, absorbing boundary which traps the line-center emission.

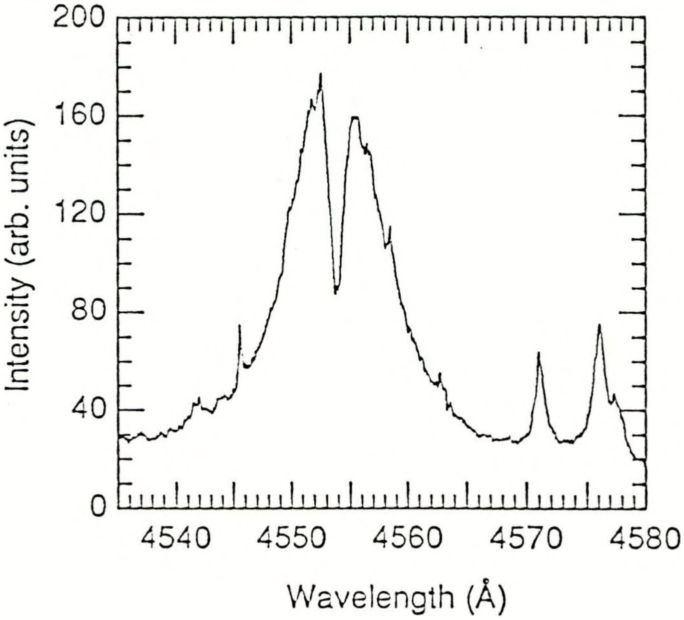

Figure 2: Spectral broadening and self absorption of the 4554 Å Ba^+ ($6p\ ^2P_{3/2} \rightarrow 6s\ ^2S_{1/2}$) resonance line fluorescence measured at $d = 1$ mm from a YBCO pellet irradiated with 3.0 J cm^{-2} at 248 nm in 10^{-6} Torr at a $\Delta\tau = 140$–200 ns following laser pulse arrival. The central portion of the spectral line is absorbed by the cooler plume surrounding the hotter central region of the plume.

Fluorescence from excited states persists to long distances in conjunction with the ions and electrons in the plume, indicating a supersonic plasma pulse with production and recombination kinetics at work in the high-density region of the plume. However, optical absorption spectroscopy reveals another, slower velocity component to the transport.[11]

This disparity is illustrated in Fig. 3 which compares the optical emission and absorption at $d = 1$ mm from a YBCO pellet in vacuum following 1 J cm^{-2} KrF irradiation. The fluorescence temporal history shows excited states of Y, Ba, and small amounts of YO, all of which are gone by 2.5 µs. Absorption of a Xe lamp continuum detects the excited states of Y and Ba, but also reveals the presence of large concentrations of ground state YO. This absorption lasts to several hundred microseconds, indicating the presence of a slow moving or stopped vapor. Similarly, optical absorption in other wavelength regions detects large densities of ground state neutrals and ions which trail the emitting plasma pulse up to several centimeters from the target.

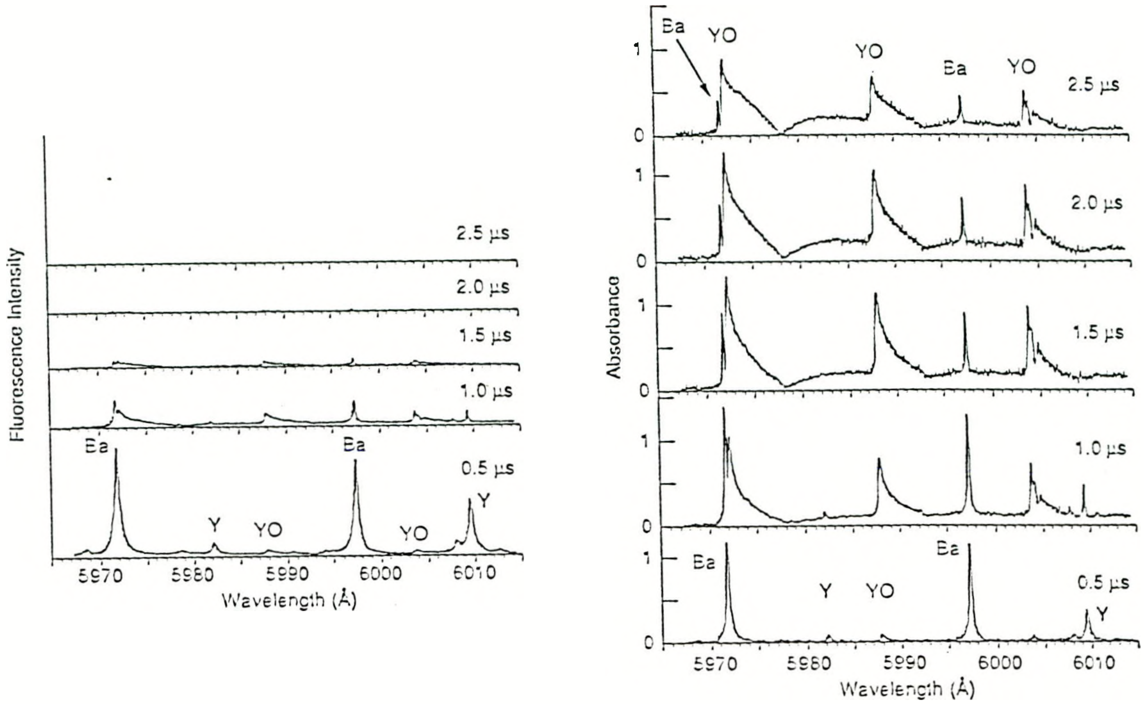

Figure 3: Fluorescence and absorption of the laser produced plasma at $d = 1$ mm from a YBCO pellet irradiated with 1.0 J cm^{-2} at 248 nm in 10^{-6} Torr. Spectra represent 200 accumulations with 20-ns temporal gate and 0.1-Å spectral resolution. While the fluorescence disappears by 2.5 µs, optical absorption reveals the presence of ground state species to much later times.

4. EXPANSION INTO BACKGROUND GASES

The YO observed in Fig. 3 may be emitted from the target in the ground state or result from gas phase conversion of Y atoms and ions. The ablation of Y metal into background oxygen results in efficient conversion of Y → YO as evidenced by an increase in fluorescence from YO (A $^2\Pi$) and absorption from YO (X $^2\Sigma$). Figure 4 illustrates this conversion process and the optical absorption technique.

At $d = 1.0$ cm and $\Delta t = 4.0$ µs, three vibrational bands of YO (A $^2\Pi \leftarrow$ X $^2\Sigma$) are clearly visible compared to the incident Xe flashlamp spectrum in Fig. 4(a). At this time and distance, the fluorescence has ended. The absorbance is calculated from $ln(I_0/I)$ where $I_0(\lambda)$ is the incident Xe lamp intensity and $I(\lambda)$ is the transmitted lamp intensity.

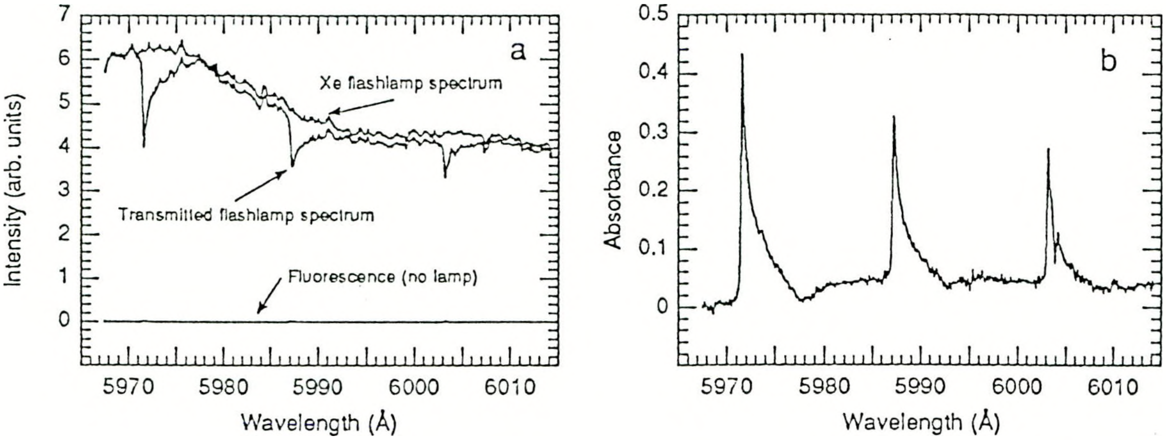

Figure 4: (a) Example of the optical absorption of a Xe flashlamp beam and the fluorescence measured at d = 1.0 cm from a Y pellet, 4.0 µs (20-ns gate) following irradiation with 1.0 J cm^{-2} at 248 nm in 200-mTorr oxygen. (b) Calculated absorbance, $ln(I_0/I)$, for the data of (a), displaying the (0,0), (1,1), and (2,2) vibrational bands of YO ($A\ ^2\Pi \leftarrow X\ ^2\Sigma$) at 5972.2, 5987.7, and 6003.6 Å, respectively.

As the background gas pressure is increased, several effects are evident. (1) The fluorescence from all species increases due to increased collision rates on the leading edge of the expansion. (2) Reactive scattering produces new gas phase species, such as the formation of YO from the ablation of Y into O_2 above. (3) The plume boundary is slowed by collisions with the background gas. (4) The amount of material penetrating the background gas is attenuated dramatically.

Figure 5 illustrates the slowing and attenuation of the expanding plasma produced by 2.5-J-cm^{-2} irradiation of YBCO into oxygen. Figure 5(a) compares seven normalized ion probe current waveforms measured at d = 5.0 cm at pressures from 0.01 to 200 mTorr. The actual magnitudes of the integrated waveforms dropped exponentially with pressure at a given distance [which can be inferred from Fig. 5(b)]. Since the ion probe is a flux sensitive detector [$F(t)=N(t)v(t)$] biased to collect positive ions, the waveforms of Fig. 5(a) are representative of the moving positive charge in the plume and not the stopped vapor.

Figure 5(a) shows the evolution of the plasma front arriving at 5.0 cm with increasing pressure. At low pressures, the plasma displays a two-component character, a fast component which is transmitted with little delay, and a component which has undergone more dramatic slowing. As the background pressure is increased, more of the plume is delayed to longer times and a single-component pulse shape is acquired past ~100 mTorr. The slowing of the plume will be discussed further below.

The total integrated positive charge transmitted versus distance for various oxygen pressures is shown in Fig. 5(b). In vacuum, the ion flux drops as $d^{-1.8}$, in near agreement with the expected d^{-2} drop for a detector of constant size

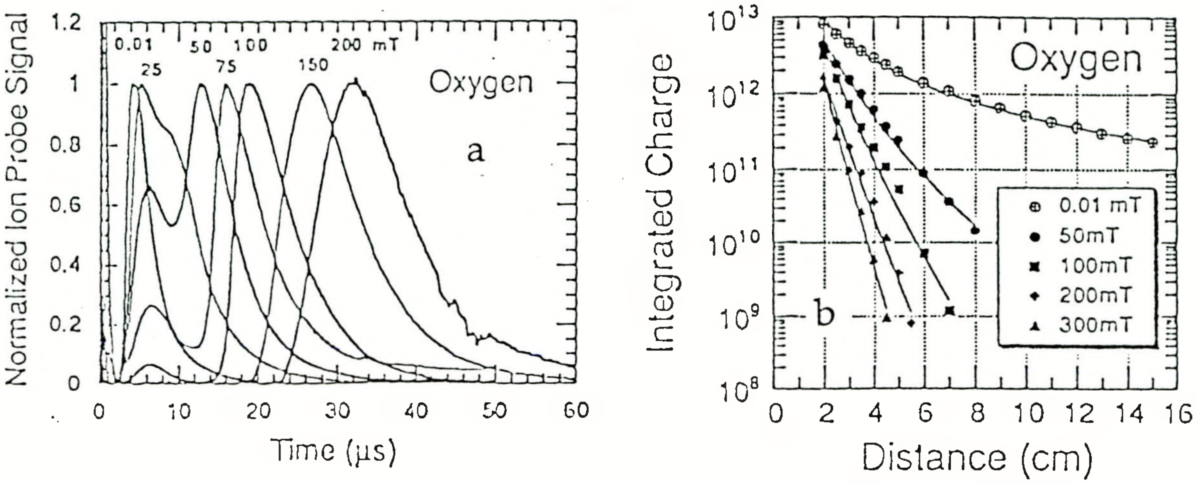

Figure 5: (a) Normalized ion probe current waveforms measured at d = 5.0 cm along the normal to a YBCO pellet irradiated with 3.0-cm^{-2} 248-nm irradiation in 0.01-, 25-, 50-, 75-, 100-, 150-, and 200-mTorr oxygen. (b) Transmitted total positive-ion charge through oxygen backpressures of 0.01, 50, 100, 200, and 300 mTorr. Fits to the data are of the form $d^{-1.8}e^{-bd}$ where b is the attenuation coefficient and d is the distance form the pellet.

at distance d from the origin of the expansion. Using the vacuum density for I_0 the attenuation of the integrated charge was fit to $I = a\, I_0\ \exp(-bd)$, where $b = N\sigma$ represents the attenuation coefficient. The attenuation coefficient was found to depend linearly on background pressure where the slope of the curve yields a general scattering cross section for ion-oxygen $\sigma_{i\text{-}O_2} = 2.3 \times 10^{-16}$ cm^2 interactions for background pressures up to 300 mTorr.[2]

For a two-dimensional view of the plume expansion into vacuum and background oxygen, the overall plume fluorescence was imaged by the gated ICCD detector at various time delays. The experimental geometry is diagrammed in Fig. 6(a). A rotating YBCO pellet is viewed side-on following irradiation by a 1.0-J-cm^{-2} KrF laser pulse (50-ns FWHM, 2 mm × 2 mm square image on the pellet surface) incident at 30°. The fast gate width of Δt = 20 ns essentially freezes the motion (at $v = 1.0 \times 10^6$ cm s^{-1}, $v\Delta t$ = 0.2 mm) of the plume in order to examine the spatial distribution of the fluorescence. Examples of expansion into vacuum [Figs. 6(b), 6(c), 6(d)] and 100-mTorr oxygen [Figs. 6(e), 6(f), 6(g), 6(h)] are presented for comparison.

In vacuum, the fluorescence begins on the surface of the pellet and then separates into two intensity regions. One part remains essentially stationary at the target surface and is gone by 2.0 μs [as in Fig. 4(a)], the other expands nearly

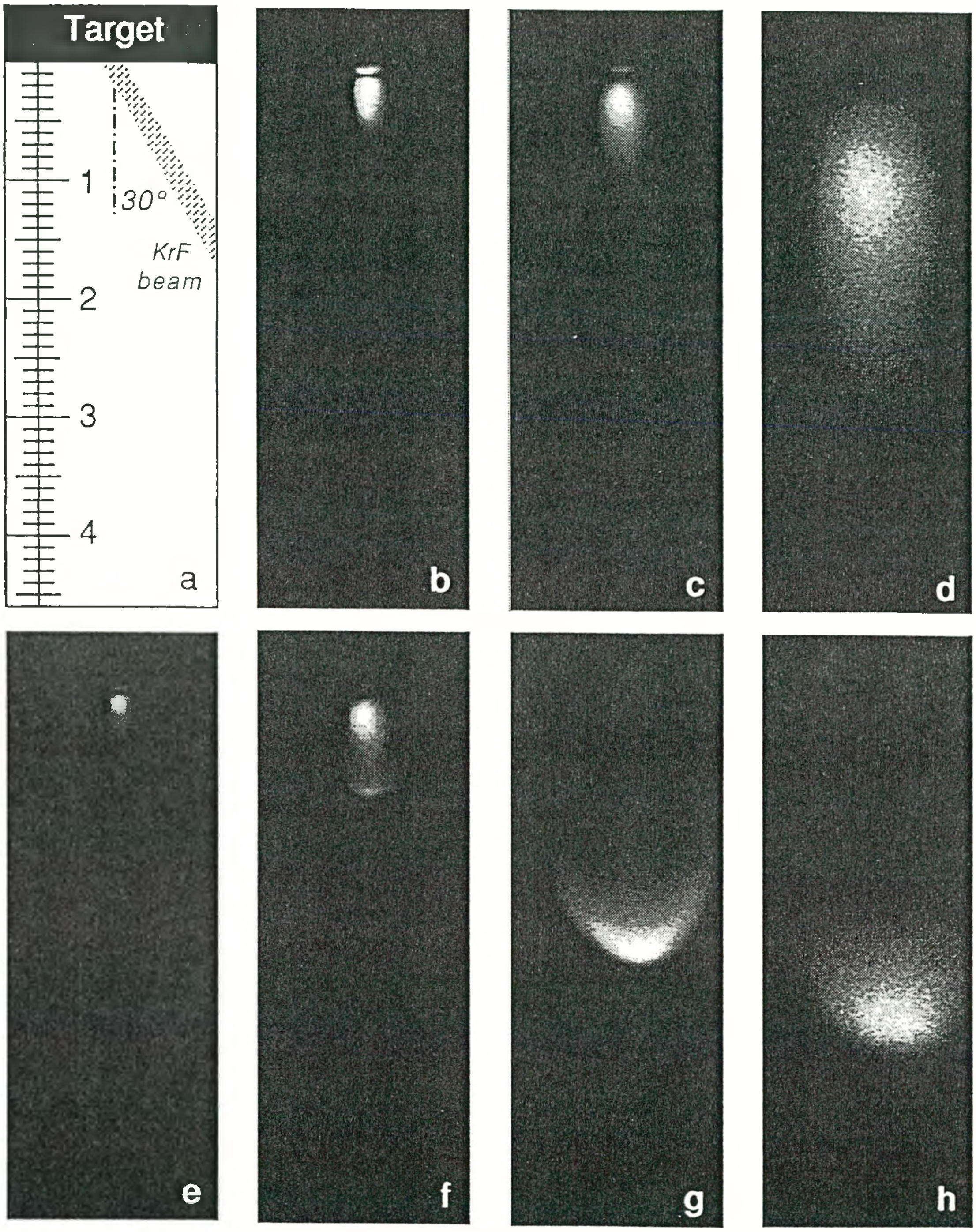

Figure 6: (a) Geometry and centimeter scale for 20-ns-gated ICCD waveforms of 1.0-J-cm^{-2} KrF/YBCO ablation in 1×10^{-6} Torr: (b) 500 ns, (c) 1.0 μs, (d) 3.0 μs and in 100 mTorr oxygen: (e) 500 ns, (f) 1.0 μs, (g) 4.0 μs, and (h) 8.0 μs.

one-dimensionally for the first 0.5 µs [Fig. 6(b)]. The leading edge of this fast component proceeds unrestricted at constant 1.0-cm-µs^{-1} velocity and the plume expands in a highly forward-directed pattern.

In 100-mTorr oxygen, expansion during the first 0.5–1.0 µs [Figs. 6(e) and 6(f)] appears nearly as unrestricted as in vacuum [Fig. 6(b) and 6(c)]. However at Δt = 1.0 µs, the fluorescence leading edge increases in intensity and begins to form a sharpened front of greater radius of curvature. From Δt = 1.0–2.0 µs, the two-component plume fluorescence coalesces into a common propagating front which is considerably slowed [Fig. 6(g)] compared to the vacuum case [Fig. 6(d)]. The plume continues to slow behind this sharp front until nearly stopped.

Position-time plots of the leading edge fluorescence (along the normal to the irradiated region) from ICCD images, including those of Fig. 6, are given in Fig. 7. In vacuum, the leading edge proceeds at constant velocity of 1.0 cm µs^{-1}. In 100-mTorr oxygen, however, it appears unaffected by the background gas for the first microsecond and then slows progressively as shown. Two curve fits to the 100-mTorr data are given in Fig. 7: (solid line) drag model $R = x_f[1 - \exp(-\beta t)]$, (dashed line) shock model $R = at^n$ with fit parameters x_f = 3.0 cm, β = 0.36 µs^{-1}, a = 0.96 cm, n = 0.57. These models will be briefly discussed below.

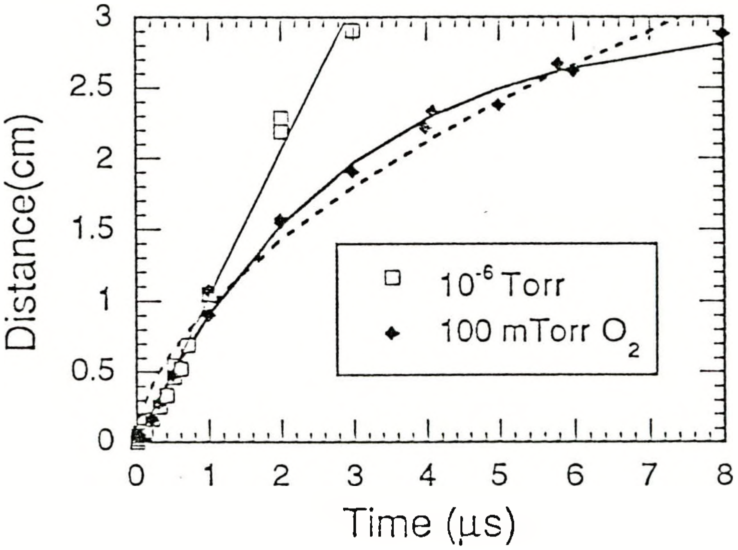

Figure 7: R-t plots of the expansion of the luminous plume along the normal to the YBCO pellet measured from gated ICCD images including those of Fig. 6. Two fits to the 100-mTorr oxygen expansion data are shown: (solid line) drag model $R = x_f[1 - \exp(-\beta t)]$, (dashed line) shock model $R = at^n$.

The development of the sharp front of fluorescence during the progression of the plasma into the gas is highly suggestive of a shock wave. For high background pressures a blast wave model[9,10] has been used to describe the target luminous shock front caused by the expansion of laser ablation plasmas.[3,9,10] This model was developed to describe the propagation of a shock wave through a background gas (density ρ_o) caused by a the sudden release of energy, E, in an explosion. The propagation of the shock front by the background gas follows the distance-time relation $R = \xi_0 (E/\rho_0)^{1/5} t^{2/5}$ where ξ_0 is a constant. This model strictly applies when the mass of the ejected products is small compared with the mass of the background gas set in motion by the shock, a situation which does not apply here.

At low pressures, such as those used for pulsed-laser deposition, fits of the form $R = at^n$ to R-t plots like Fig. 7 require exponents >0.4 ($n = 0.57$ in Fig. 7) for satisfactory agreement. Fits to $R = at^{0.4}$ consistently predict greater propagation distances than actually measured at early times. Ignoring the region in time prior to the observed formation of the shock front, the blast wave model describes the later stages of the expansion increasingly well at higher background pressures.

A classical drag force model shows better agreement at low pressures (solid line in Fig. 7). The ejected pulse of ablation products is regarded as an ensemble which experiences a viscous force proportional to its velocity through the background gas. The equations of motion are given by

$$a = -\beta v \qquad \text{giving}$$
$$v = v_0 \exp(-\beta t) \qquad v = \beta(x_f - x)$$
$$x = x_f [1 - \exp(-\beta t)] \qquad a = -\beta^2 (x_f - x)\,,$$

where β is the slowing coefficient and $x_f = v_0/\beta$ is the stopping distance of the plume.

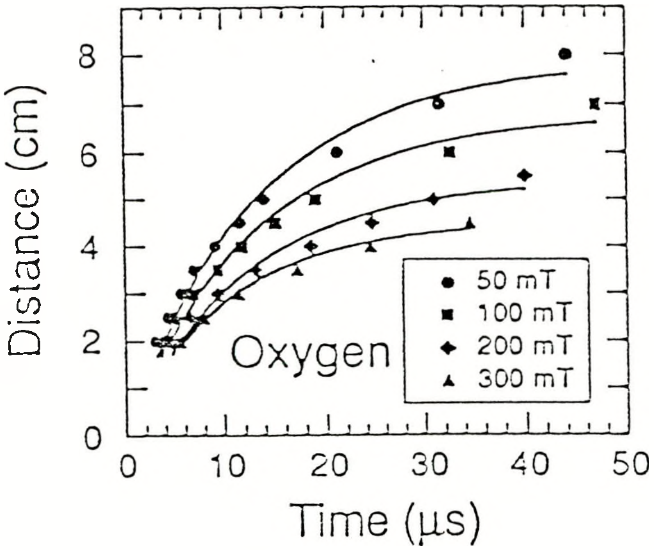

Figure 8: Position-time plots of the plasma propagation through background oxygen following 2.5-J-cm^{-2} KrF irradiation. Points represent arrival times of the peak of the positive ion flux from a Langmuir probe. Fits to the curves are of the form $R = x_f [1 - \exp(-\beta t)]$ where: x_f = 7.9, 6.8, 5.4, and 4.5 cm and β^{-1} = 13.0, 12.9, 12.1, and 10.2 µs, for 50, 100, 200, and 300 mTorr, respectively.

The drag model predicts that the plume will eventually come to rest, due to resistance from collisions with the background gas. However, from both ion probe and fluorescence data such as Fig. 7, the ranges predicted are somewhat too short.

Ion probe data give similar results. Figure 8 maps the propagation of the peak of the ion probe current pulse for oxygen pressures of 50, 100, 200, and 300 mTorr along the normal to the pellet following 2.5-J-cm^{-2} KrF irradiation. While the overall fits to the data are better represented by the drag model, the plume is found to overshoot the predicted range and continue propagating more like a shock wave. The shock model for the same data yielded best-fit values of the power law exponent varying from 0.54 at 50 mTorr to 0.45 at 300 mTorr, suggesting a better agreement at higher pressures.

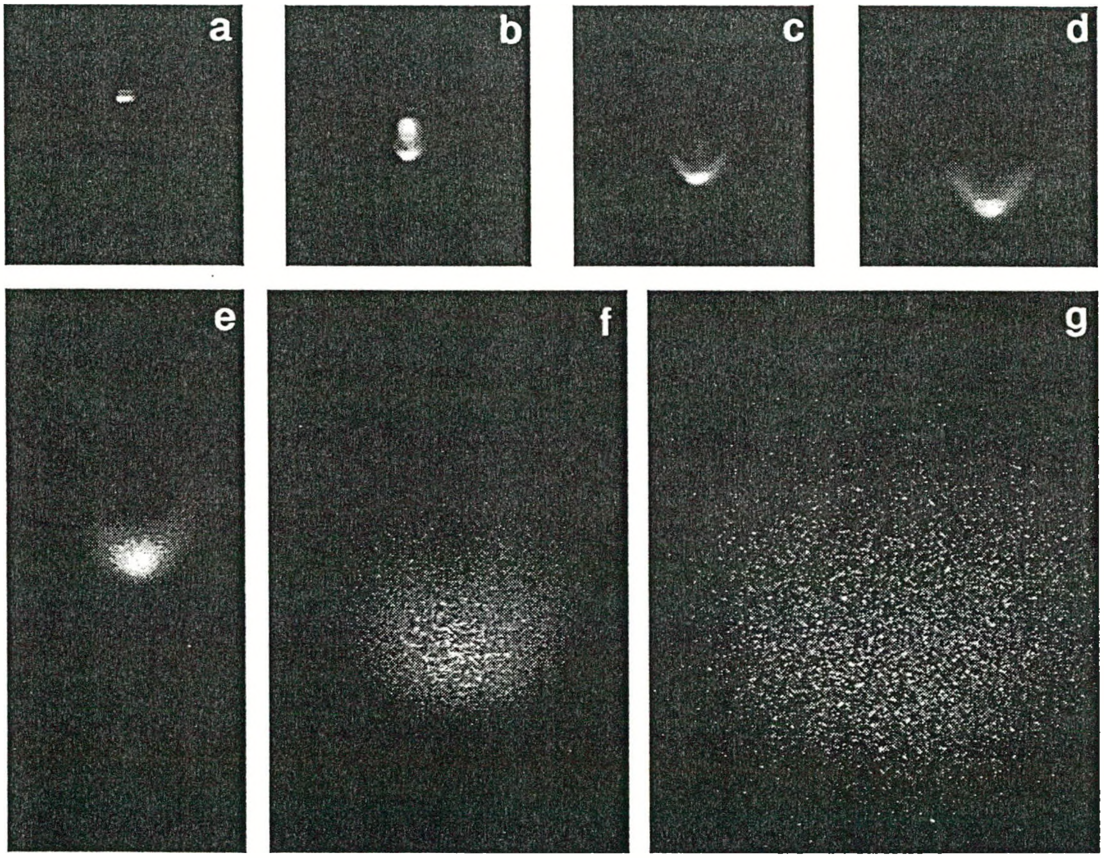

Figure 9: Gated ICCD images of the expansion of 1.0-J-cm^{-2} KrF-irradiated YBCO into 200mT Xe background gas at (a) 100 ns, (b) 500 ns (c) 1.0 μs, (d) 2.0 μs, (e) 5.0 μs, (f) 20 μs, and (g) 300 μs.

Utilizing the same geometry of Fig. 6, gated ICCD images were taken at various time delays during the plasma propagation following 1.0-J-cm^{-2} ablation of YBCO into 200-mTorr Xe. The results are shown in Fig. 9. Very similar shock formation behavior was observed in xenon, however there were also several differences. The stationary plasma at the pellet was again evident and lasted to only 1.0 μs. In the higher pressure, higher mass xenon; the leading edge begins to form an extended frontal shock boundary after only 500 ns, as shown in Fig. 9(b). Over a smaller temporal and spatial window, the fluorescence settles from a two-component plasma to a well-defined front which moves out and essentially stops.

Two distance-time plots for the propagation of the leading edge of the plasma propagation are given in Fig. 10. Curve fits to the drag and shock models over the 0–10 μs time interval are given in Fig. 10(a) and redrawn in Fig. 10(b) which shows the position of the nearly stationary plume boundary at late times. Neither model is capable of describing the position at both early and late times; however the shock model appears to better describe the data than the drag model during the early time period.

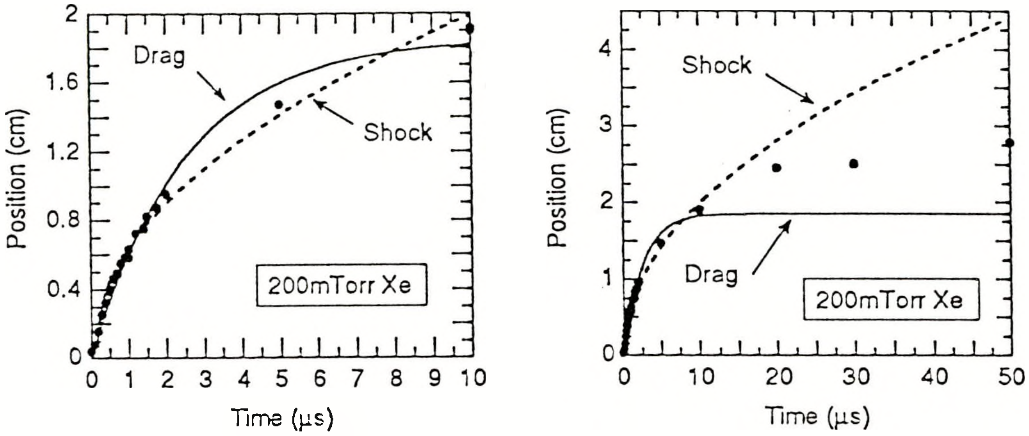

Figure 10: *R-t* plot of the expansion of the luminous plume along the normal to the YBCO pellet measured from gated ICCD images including those of Fig. 10. Two fits to the 200-mTorr xenon expansion data are shown: (solid line) drag model $R = x_f(1 - \exp(-\beta t))$, (dashed line) shock model $R = at^n$.

The combined indications of the ICCD images and the ion probe data are that during the initial stages of expansion, while the mass of plume ejectants exceeds the mass of gas it has displaced, the plume propagates through the background gas in agreement with a drag model, experiencing little slowing until a critical point at which a visible shock structure starts to form. During this transition region in space and time, the plasma appears to have two components, an initial fast component which has traveled at nearly the vacuum speed and a delayed component which arrives later. This behavior is seen by both ion probe and fast photography. At longer distances and times, a single component shock structure remains to propagate in better agreement with the shock model.

To investigate the validity of the shock propagation model following the transition region, a set of ion probe waveforms were taken at 2, 3, 4, and 5 cm following 2.5-J-cm^{-2} ablation of YBCO in 200-mTorr oxygen. The shape of the entire positive ion pulse arriving at 3, 4, and 5 cm was modeled based upon the 2-cm waveform and the shock and drag models. The data are the solid curves in Fig. 11.

The ion probe current at a given time t results from the incident flux $N(t)v(t)$ at that moment, where $N(t)$ is the number density and $v(t)$ is the velocity. From the arrival times at $d = 2$ cm and the shock relation $v(x,t) = nx/t$, the number density and corresponding velocity $N_2(t)$ and $v_2(t)$ were separately determined according to the shock model. The arrival times and velocities of the 2-cm number density, $N_2(t_2)$, were determined at subsequent distances by the relations: $v_j = v_2\,(x_j/2)(t_2/t_j)$ where $t_j = t_2\,(j/2)^{1/n}$. The modeled flux downstream, $N_2(t_j)\,v_j$ was then constructed for comparison with the measured current. The power law exponent, , was iterated to determine the best fit to the 5 cm waveform. The results are shown by the dashed lines in Fig. 11. The value of the best-fit exponent is $n = 0.49$.

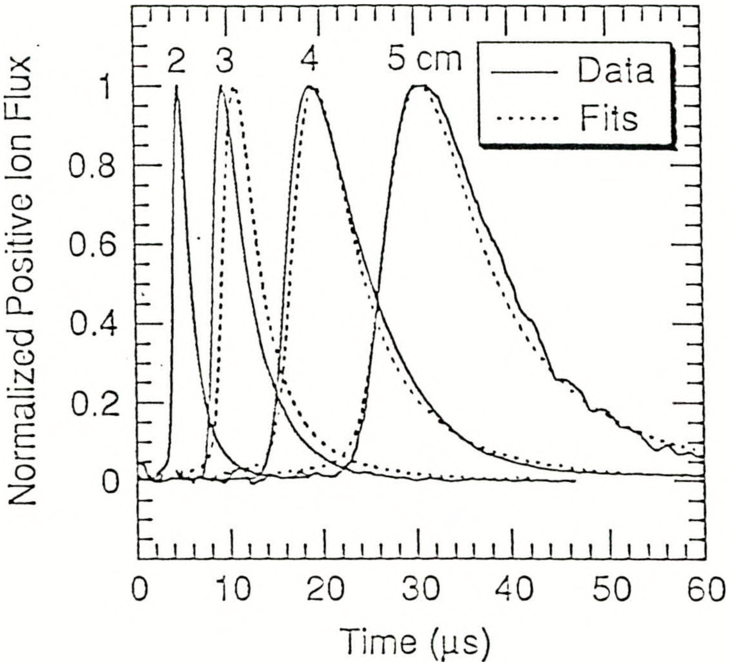

Figure 11: Normalized ion probe waveforms (solid lines) at 2, 3, 4, and 5 cm normal to a YBCO target irradiated with 2.5 J cm^{-2} at $\lambda = 248$ nm in 200-mTorr oxygen illustrating the delay and broadening of ion flux arrival times due to thermalization of the plume. The dashed lines are the ion fluxes simulated by propagating the 2-cm waveform to 3, 4, and 5 cm with a shock propagation model where the position evolves as $R = at^{0.49}$.

The results of Fig. 11 show that the entire shape of the pulse of positive ions is well represented by a power-law-dependence shock propagation model for the higher background oxygen pressures in the film growth regime.

4. SUMMARY AND CONCLUSIONS

The propagation of the plume of KrF-laser-ablated material from a YBCO target into background gas pressures used for film growth has been studied by fast gated ICCD photography, ion probe measurements, and high-resolution optical emission and absorption spectroscopy. Fast ion probes sensitive to the flux of positive ions reveal that the ions are attenuated exponentially with distance and pressure, in accordance with a simple scattering model which yields an overall ion-oxygen reaction cross section of $\sigma_{i\text{-}O_2} = 2.3 \times 10^{-16}\ \mathrm{cm}^2$ for oxygen pressures up to 300 mTorr.

Sensitive ICCD photography permitted the evolution of the shock front in background oxygen and xenon to be traced with 5-ns temporal resolution. The results show several interesting effects. First, the initial plasma at the pellet surface separates into a nearly stationary section within 1 mm of the pellet surface and an expanding component which initially undergoes a one-dimensional expansion in vacuum and background gases for a given distance, followed by a 3-dimensional expansion in vacuum.

Second, in background gases, the plume undergoes a transition in space and time during the formation of a shock front. During this transition region, the plasma appears to have two components, an initial fast component which has traveled at nearly vacuum speed and a delayed component. Ion probe waveforms show these two components and the disappearance of the fast component as the shock front consolidates.

At the lower pressures investigated here, the propagation of the plume agrees with a drag model during the initial expansion, when the mass and pressure of the plume material are greater than that of the gas with which it has interacted. This model predicts the eventual stopping of the plume due to a viscous drag force.

As the pressure and/or distance are increased, a consolidated shock front is evident from ICCD photography, optical emission and absorption spectroscopy, and ion probe measurements. This shock front contains the ablation products, in contrast to the blast wave model which follows a pressure disturbance through the gas itself. The power-law dependence form of the shock propagation model, however, appears to describe the propagation of this shock front and, in fact, the shape of the entire positive ion waveform. The value of the power-law exponent, $n = 0.49$ for 200 mTorr oxygen, is greater than that predicted by blast wave theory.

Optical absorption spectroscopy reveals high densities of non-emitting neutrals and molecules at times much greater than the plume fluorescence at distances up to several centimeters from the pellet. Large densities of YO are formed or ejected at later times in vacuum close to the pellet and are found to result from reactive collisions of ablated yttrium with oxygen far from the pellet. Reactive collisions such as this are partly responsible for the measured attenuation of the positive ions and the increase in fluorescence observed on the ICCD photographs.

The combined set of in situ diagnostics (ion probes, optical emission spectroscopy, optical absorption spectroscopy, and ICCD photography) allows several views of the ions, excited states, and ground states in the plume which are necessary to optimize the gas phase conditions necessary for applications such as thin-film growth and cluster formation.

5. ACKNOWLEDGEMENTS

The assistance and experimental expertise of Hollis Davis and Yair Talmi of Princeton Instruments, Inc., during their loan of the gated, intensified ICCD detector are deeply appreciated. This research was supported by the Division of Materials Sciences, U.S. Department of Energy under contract DE-AC05-84OR21400 with Martin Marietta Energy Systems, Inc.

6. REFERENCES

1. J. P. Zheng, Z. Q. Huang, D. T. Shaw and H. S. Kwok, *Appl. Phys. Lett.* **54**, 280 (1989).
2. D. B. Geohegan, p. 557 in *Surface Chemistry and Beam-Solid Interactions*, Materials Research Society, Pittsburgh, Pennsylvania (1990).
3. P. E. Dyer, A. Issa, and P. H. Key, *Appl. Surf. Sci.* **46**, 89 (1990).
4. A. Gupta, B. W. Hussey, A. Kussmaul and A. Segmuller, *Appl. Phys. Lett.* **57**, 2365 (1990).
5. K. Scott, J. M. Huntley, W. A. Phillips, John Clarke, and J. E. Field, *Appl.Phys.Lett.* **57**, 922 (1990).
6. D. B. Geohegan, p. 15 in *Workshop on Laser Ablation–Mechanisms and Applications*, Oak Ridge, Tennessee, April 8–10, 1991, (in press).
7. C. Girault, D. Damiani, J. Aubreton, and A. Catherinot, *Appl. Phys. Lett.* **54**, 2035 (1989).
8. J. P. Zheng, Q. Y. Ying, S. Witanachchi, Z. Q. Huang, D. T. Shaw, and H. S. Kwok, *Appl. Phys. Lett.* **54**, 954 (1989).
9. Ya. B. Zel'dovich and Yu. P. Raizer, p. 94. in *Physics of Shock Waves and High-Temperature Hydrodynamic Phenomena*, Vol. 1,Academic Press, New York, 1966.
10. M. A. Liberman and A. L. Velikovich in *Physics of Shock Waves in Gases and Plasmas*, Springer-Verlag, Berlin, 1986.
11. D. B. Geohegan and D. N. Mashburn, *Appl. Phys. Lett.* 55, 2345 (1989).